


Provided for non-commercial research and education use.
Not for reproduction, distribution or commercial use.

Volume A877, 1 March 2012		ISSN 0375-9474
	NUCLEAR PHYSICS A	
Nuclear and Hadronic Physics		
<small>Journal devoted to the experimental and theoretical study of the fundamental constituents of matter and their interactions. Abstracted/Indexed in: Current Contents: Physical, Chemical & Earth Sciences. Also covered in the abstract and citation database SciVerse Scopus®. Full text available on SciVerse ScienceDirect®</small>		
Supervisory Editors: A. Gal, R. Hayano, J. Jolie, K. Langanke, L. McLerran, M. Soyeur, J. Stachel, M. Thoennessen		
NUCLEAR STRUCTURE AND DYNAMICS	K.P. Santhosh, J.G. Joseph and B. Piyanka <i>Fine structure in the α-decay of odd-even nuclei</i>	1
	K.A. Gladishki, P. Petkov, A. Dewald, C. Fransen, M. Hackstein, J. Jolie, Th. Piesulla, W. Rother and K.O. Zell <i>Yrast electromagnetic transition strengths and shape coexistence in ^{162}Pt</i>	19
	E. Yüksel, E. Khan and K. Bozkurt <i>Analysis of the neutron and proton contributions to the pygmy dipole mode in doubly magic nuclei</i>	35
	Z.X. Xu, C. Qi, J. Blomqvist, R.J. Liotta and R. Wyss <i>Multisite shell model description of spin-aligned neutron-proton pair coupling</i>	51
	M.I. Jaghoub and G.H. Rawitscher <i>Evidence of nonlocality due to a gradient term in the optical model</i>	59
HADRONIC PHYSICS AND HIGH ENERGY QCD	T. Kojo <i>A (1+1)-dimensional example of Quarkyonic matter</i>	70
INTERMEDIATE AND HIGH ENERGY HEAVY ION PHYSICS	F. Akram and M.A.K. Lodhi <i>B₁ absorption cross sections by nucleons</i>	95
Honorary Editor: G.E. Brown		Available online at www.sciencedirect.com SciVerse ScienceDirect

This article appeared in a journal published by Elsevier. The attached copy is furnished to the author for internal non-commercial research and education use, including for instruction at the authors institution and sharing with colleagues.

Other uses, including reproduction and distribution, or selling or licensing copies, or posting to personal, institutional or third party websites are prohibited.

In most cases authors are permitted to post their version of the article (e.g. in Word or Tex form) to their personal website or institutional repository. Authors requiring further information regarding Elsevier's archiving and manuscript policies are encouraged to visit:

<http://www.elsevier.com/copyright>



Yrast electromagnetic transition strengths and shape coexistence in ^{182}Pt

K.A. Gladnishki^{a,b}, P. Petkov^{a,c,*}, A. Dewald^a, C. Fransen^a,
M. Hackstein^a, J. Jolie^a, Th. Pissulla^a, W. Rother^a, K.O. Zell^a

^a Institut für Kernphysik, Universität zu Köln, D-50937 Köln, Germany

^b Faculty of Physics, St. Kliment Ohridski University of Sofia, 1164 Sofia, Bulgaria

^c Bulgarian Academy of Sciences, Institute for Nuclear Research and Nuclear Energy, 1784 Sofia, Bulgaria

Received 2 October 2011; received in revised form 30 December 2011; accepted 2 January 2012

Available online 10 January 2012

Abstract

Using the reaction $^{170}\text{Yb}(^{16}\text{O}, 4n)$ at a beam energy of 87 MeV and the Recoil Distance Doppler-Shift Method, five lifetimes in the yrast band of ^{182}Pt have been determined for the first time. For the data analysis, a dedicated version of the Differential Decay Curve Method has been employed. Calculations within the Interacting Boson Model and the General Collective Model indicate shape coexistence in the investigated nucleus.

© 2012 Elsevier B.V. All rights reserved.

Keywords: NUCLEAR REACTIONS $^{170}\text{Yb}(^{16}\text{O}, 4n)$, $E = 87$ MeV; measured E_γ , $I_\gamma(\theta)$, $\gamma\gamma$ -coin; deduced yrast band $T_{-1/2}$, transition quadrupole moment, $B(E2)$; calculated levels, J , π , quadrupole moment, deformation, shape coexistence, $B(E2)$. Recoil distance Doppler shift; Differential decay curve method; General collective model; Extended consistent Q-formalism; IBM-1. Comparison with data

1. Introduction

Even–even nuclei close to the proton shell closure at $Z = 82$ are a subject of numerous experimental and theoretical studies. One of the challenges for these studies is the understanding of the shape evolution in the isotopic chains when the number of the protons approaches magicity.

* Corresponding author at: Bulgarian Academy of Sciences, Institute for Nuclear Research and Nuclear Energy, 1784 Sofia, Bulgaria.

E-mail address: petkov@inrne.bas.bg (P. Petkov).

Suggested by the spectroscopic properties of the corresponding level schemes, phenomena as shape coexistence and shape transitions are commonly believed to occur. The origin of shape coexisting structures is related to excitations across the shell gap, which lead through the residual proton–neutron interaction to the lowering of deformed bands in addition to the “normal” spherical states (cf. e.g. [1]). The most popular example of this effect is ^{186}Pb , where 0^+ band-heads of prolate and oblate character were found close in energy to the spherical 0^+ ground-state [2]. The phenomenon of shape coexistence is also revealed by the properties of the nuclei from the Pt isotopic chain. Many theoretical calculations suggest a scenario for a shape evolution which includes the presence of prolate intruder states related to proton excitations across the shell gap coexisting with near-spherical or somewhat oblate states (see e.g. Refs. [3–7] and references therein). Experimental evidence of the mixing of bands with different deformations is also available [8–10]. However, other theoretical approaches, while not excluding shape coexistence, provide a good description of the spectroscopic properties without the inclusion of intruder states. Thus, IBM-1 calculations within the Extended Consistent Q -Formalism (ECQF) describe reasonably the level energies and the $B(E2)$ transition strengths of the even–even Pt isotopes [11]. From that point of view, the debate about shape coexistence in these nuclei requires new experimental data and new calculations to ensure arguments for a consensus or for a refinement of the discussion [12,13].

This situation motivated our study of ^{182}Pt , the mid-shell nucleus with 104 neutrons where the ground-state band and low-lying excited 0_2^+ and 2_2^+ bands complement the picture of collective excitations below and in the region of the pairing gap. Spectroscopic information on the level scheme of this nucleus was accumulated during the years (cf. [14,15] and references therein), but data on absolute transition probabilities were missing. Therefore we decided to carry out Recoil Distance Doppler-Shift (RDDS) lifetime measurements for the yrast band at the FN Tandem of the University of Cologne. To analyze the data, it was found necessary to modify the existing procedure of the Differential Decay Curve Method (DDCM) [16,17] in order to take into account effects as relatively small Doppler-shifts of the γ -ray transition energies and recoils stopped already in the target. An additional motivation for our study was the opportunity to apply the contemporary version (cf. [18,19] and references therein) of the General Collective Model (GCM) [20] for the description of the spectroscopic properties and use the derived collective potential $V(\beta, \gamma)$ and wave functions for a visualization of the underlying nuclear shapes. It should be mentioned that the GCM was already used for the description of some heavier Pt isotopes [21] and it is interesting to compare the results from an application to ^{182}Pt with calculations using other theoretical approaches. Finally, in the region of Os isotopes with $A \approx 180$, a new island of X(5)-like [22] nuclei has been recently found [23]. It is of interest to establish the limits of this island on the nuclear landscape, as well as to investigate for possible remnants of the X(5) structure in neighboring nuclei. These topics will be covered by the following presentation. First, the RDDS experiment is presented followed by the procedure for the data analysis and the results. Then, the spectroscopic properties, including the newly derived $B(E2)$ transition strengths, and the shape coexistence are discussed in the terms of GCM and IBM calculations performed by us as well as of the predictions of other theoretical models. At the end, some conclusions are made.

2. Experiment

To populate excited states in ^{182}Pt , we used the reaction $^{170}\text{Yb}(^{16}\text{O}, 4n)$. The beam, with an energy of $E = 87$ MeV, was provided by the FN Tandem of the Institut für Kernphysik of the Universität zu Köln. The target consisted of 1.0 mg/cm² isotopically enriched ^{170}Yb evaporated onto a 2.1 mg/cm² Ta foil serving as a backing and facing the beam. After a flight in

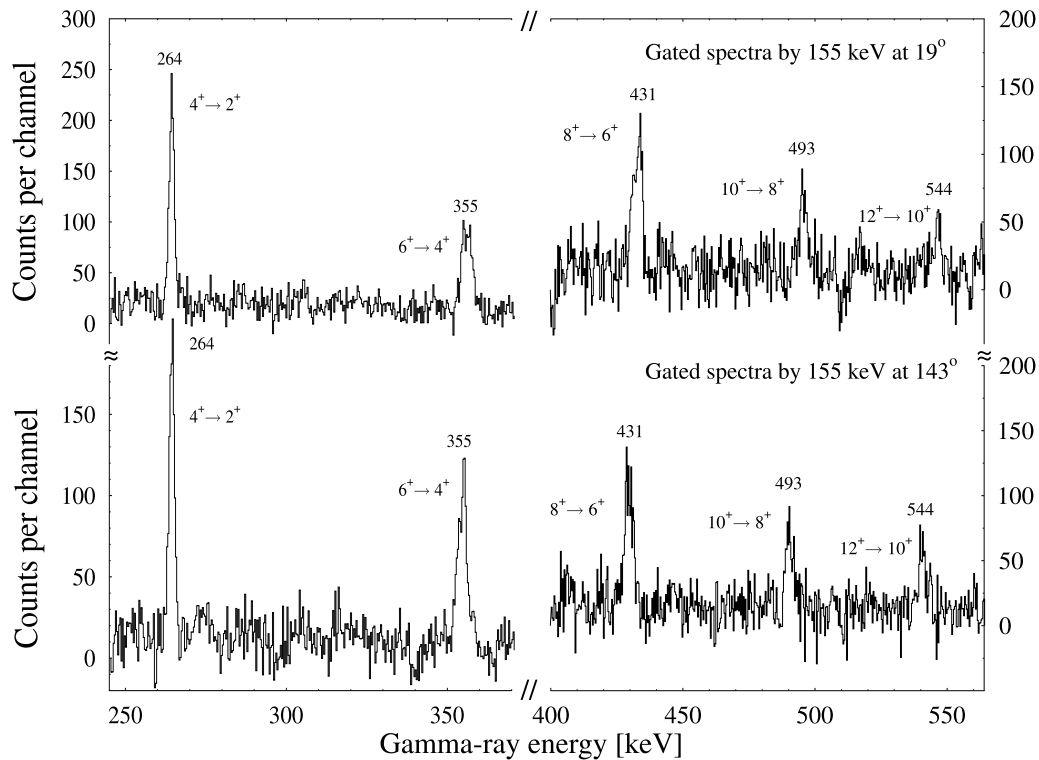


Fig. 1. Examples of RDDS spectra taken at the distance of $26 \mu\text{m}$ with the detectors of rings 1 and 2. The gate is set on the 155 keV ground-state transition. See also Ref. [15] and Fig. 4 in Section 4.

vacuum with a mean velocity of about 0.63% of the velocity of light, c , the recoiling nuclei were stopped in a 3.5 mg/cm^2 gold foil. The Yb/Ta and Au foils were mounted in the Cologne plunger apparatus [24] where the constancy of the selected target-to-stopper distance is controlled by measuring the target–stopper capacity and by compensating drifts with a piezo-electric device. The distances are set by moving the target holder. Coincident deexciting γ -rays were recorded with a setup consisting of five large volume germanium detectors positioned symmetrically at the backward angle of 143° and a Euroball cluster [25] detector positioned at 0° with respect to the beam axis. The germanium crystals used were grouped in three rings, namely ring 2 (polar angle of 143° with respect to the beam axis), ring 1 (outer cluster segments at a polar angle of 19°) and ring 0 (central segment of the cluster at 0°). Data were taken for 10 target-to-stopper distances x in the range from $3.0 \mu\text{m}$ to $1500 \mu\text{m}$. A total of about 3.0×10^9 unfolded double events were collected. After corrections for energy shifts and gain matching, the data were sorted into $80 \text{ } 8k \times 8k$ γ - γ coincidence matrices. Each matrix contains events where two γ -rays are registered by detectors belonging to a particular two-ring combination (out of 8 possible because ring 0 consists of only one detector) at a given distance. The normalization of the data taken at different target-to-stopper distances was performed using coincidence events corresponding to pairs of strong transitions in the yrast band (cf. Ref. [24]). Examples of spectra taken at backward and forward angles at the distance of $26 \mu\text{m}$ are shown in Fig. 1.

3. Data analysis and results

The RDDS method is a well known technique for the determination of picosecond lifetimes of excited nuclear states (for a detailed presentation see e.g. Ref. [26] and references therein). It uses the timing information involved in the splitting of the intensity of a depopulating γ -

ray transition into components characterized by a different Doppler-shift. The γ -rays emitted in flight by the nuclei recoiling from the target are detected with a Doppler-shifted energy and give rise to the shifted (S -) component or peak in the spectrum. Emissions occurring at rest in the stopper contribute to the unshifted (U -) component. The evolution of the intensity splitting which follows the change of the target-to-stopper distance is sensitive with respect to the lifetime τ of the depopulated level. Therefore the determination of the areas of the U - and S -peaks is of primary importance for the analysis of RDDS data.

The precision of this determination, however, can be hindered by several factors. These factors were considered in detail in Ref. [27]. Here we only mention the main points which are relevant for the present measurement. The most commonly encountered difficulty arises when the two peaks are not well separated e.g. due to a small Doppler shift as in our case. Then, their line-shapes have to be known in order to disentangle the U - and S -contributions. The shape of the U -peak is described by the response function of the detector, but the shape of the S -peak depends also on the corresponding velocity distribution of the recoiling nuclei which is determined by the target thickness and stopping powers, reaction kinematics and beam energy. Additionally, the shape of the S -peak is to some extent distance-dependent since the faster recoils reach the stopper in a shorter time than the slower ones and therefore contribute less to the S -peak, especially at short distances. In our experiment, due to the relatively low recoil velocity and large target thickness, about 25% of the recoils were already stopped in the target as empirically proved by analyzing the areas of the persisting unshifted peaks at very large distances for short lived levels. This effect has to be taken into account in the analysis. Finally, the recoiling nuclei need a finite time interval (typically about 1 ps) to come to rest in the stopper and during the slowing-down, the Doppler-shift of the emitted γ -rays is attenuated which gives rise to a continuous (DSA) spectrum.

In Ref. [27], a solution of these experimental problems was proposed for the case of coincidence RDDS measurements where a gate is set on the shifted component of a transition directly feeding the level of interest. In the present work, due to the relatively small Doppler-shifts of the transitions of interest, it was not possible to use such gating without a significant loss of statistics. The point is that the gate must not include the unshifted peak of the feeding transition and therefore has to be set on the very high-velocity part of the shifted peaks which leads to less counts in the gated spectra. Therefore we used the procedure [27] but in a variant [28] which is relevant for a case where the gating condition does not influence the timing information for the investigated level. Namely, in order to deduce the intensities of the transition of interest and of a feeding transition, gates were set on the complete line (both shifted and unshifted components included) of the feeding transition and of the transition of interest, respectively. In this way, the problem with the unknown (unobserved) feeding was solved by using coincidences of a feeding transition with the transition of interest. To increase statistics, we summed up the spectra corresponding to gates set in the three independent rings.

To check for possible deorientation effects (see e.g. Ref. [29]), we considered the behavior of the sum of the shifted and unshifted components as function of the target-to-stopper distance. No deviation from a constant behavior was found within the error bars. Therefore we conclude that the present results are not affected by the deorientation and give a conservative estimate of 5% from the values of the derived lifetimes as a possible influence of the deorientation which might lead to larger lifetimes due to the stretched character of the investigated E2 transitions.

As discussed in Ref. [28], after the creation of the excited nucleus at time $t = 0$, the transition of interest can occur in four physically distinct cases: during the motion in the target finishing

at t_{fi} , the flight in vacuum which ends at t_{ff} , the slowing-down in the stopper completed at t_s and after coming to rest. Correspondingly, four different components contribute to the spectrum.

To apply in practice the formalism of Ref. [28], we performed a Monte Carlo (MC) simulation in three dimensions of the time evolution of the velocity distribution of the recoils by describing the processes of the creation of the recoils, slowing-down in the target, free flight in vacuum and slowing-down in the stopper. Further, the “velocity histories” were randomized with respect to the registering detectors. A modified version of the computer code DESASTOP [27,30] was used for the Monte Carlo simulation. Details about the code and more specifically, the treatment of the electron and nuclear stoppings can be found in Ref. [31]. We only mention here that the electron stopping power $(\frac{d\epsilon}{d\rho})_e$ is described by a formula [32] which generalizes the theory [33] of Lindhard, Scharff and Schiøtt (LSS). In the corresponding dimensionless units, it reads

$$\left(\frac{d\epsilon}{d\rho}\right)_e = f_e k_{LSS} \epsilon^a \quad (1)$$

where k_{LSS} is a constant given by the theory. For the ^{182}Pt ions in the ^{170}Yb target we used $f_e = 1.108$ and $a = 0.625$, while for the gold stopper, the values were $f_e = 0.490$ and $a = 0.620$. These parameters were derived according to the procedure outlined in Ref. [31] from the semi-empirical tables of Northcliffe and Schilling [34] with taking into account effects of the medium atomic structure [35,36]. For the nuclear stopping power a reduction factor f_n was treated as an adjustable parameter and a value of 0.7 was adopted as suggested in Refs. [36,37]. At large distances, the line-shapes of the shifted peaks were satisfactorily reproduced and therefore one can conclude that the stopping powers of the target material were correctly taken into account. We remind that only at large distances these line-shapes are fully representative for the underlying velocity distribution of the recoiling nuclei. Concerning the slowing-down in the stopper, the mean time interval needed by the recoils to come to rest is predicted to be about 0.8 ps while the whole process is fully completed within some 1.6 ps. A summation over several thousands MC-histories is sufficient for a determination of the line-shapes. In the procedure for the analysis, the background-subtracted line-shapes corresponding to the transition of interest at all distances and the shifted decay curve

$$S_{af}(t) = b_{af} \int_0^t \lambda_a n_a(t') dt', \quad (2)$$

are fitted simultaneously. The “unshifted” decay curve is given by the complementary integral:

$$R_{af}(t) = b_{af} \int_t^\infty \lambda_a n_a(t') dt' = S_{af}(\infty) - S_{af}(t). \quad (3)$$

In Eqs. (2), (3), $n_a(t)$ is the time-dependent population of the level of interest a , λ_a is its decay constant (the lifetime $\tau_a = 1/\lambda_a$) and b_{af} is the branching ratio of the transition $a \rightarrow f$. For the analysis, the function $S_{af}(t)$ is represented by continuously interconnected second-order polynomials over an arbitrarily chosen set of neighboring time-intervals. The fitting problem is linear with respect to the polynomial parameters and the areas of the unshifted peak. The fitting procedure is performed by changing the limits of the time-intervals until the best reproduction of the spectra is achieved. It should be noticed that we tried first to fit by a single Gaussian the unshifted peak which contains contributions from emissions at rest in the stopper and in the target. This approach did not give good results and we modified the code to calculate and involve in the fit,

Table 1

Lifetimes and reduced electromagnetic transition probabilities in the yrast band of ^{182}Pt derived in this work. The level energy and its spin/parity are displayed in columns 1 and 2, respectively. The next column shows the energy of the depopulating γ -ray transition. In the fourth column, the derived lifetime is displayed. The reduced transition probabilities $B(E2)$ are shown in e^2b^2 and in Weisskopf units. The last column presents the transition quadrupole moments Q_t .

E_{lev} [keV]	I^π	E_γ [keV]	τ [ps]	$B(E2)$ [e^2b^2]	$B(E2)$ [W.u.]	Q_t [eb]
155.0	2 ⁺	155	590 (102)	0.816 (143)	133 (23)	6.40 (56)
419.6	4 ⁺	264	44 (5)	1.255 (143)	205 (23)	6.65 (38)
774.9	6 ⁺	355	7.4 (6)	1.843 (150)	301 (24)	7.67 (31)
1205.8	8 ⁺	431	2.7 (5)	1.963 (364)	321 (59)	7.74 (72)
1698.4	10 ⁺	493	1.3 (3)	2.110 (487)	344 (80)	7.92 (91)

using the knowledge of $S_{af}(t)$ (and $R_{af}(t)$), the contribution from nuclei stopped already in the target.

For singles-like RDDS measurements, the DDCM [16] provides an expression for the lifetime of the level of interest τ_a at every distance x or flight time $t = x/v_z$:

$$\tau_a(t) = \left(R_{af}(t) - b_{af} \sum_{h=1}^N (1 + \alpha_{ha}) R_{ha}(t) \right) / (b_{af} \lambda_a n_a(t)). \quad (4)$$

The numerator yields the number of nuclei $n_a(t)$ at time t which decay via the transition $a \rightarrow f$ (cf. Ref. [16]). The quantities α_{ha} are the internal conversion coefficients of the γ -ray transitions $h \rightarrow a$ and the sum runs only over the direct feeders h of the level a . The denominator represents the first derivative of the shifted decay curve $S_{af}(t)$ or the decay function of the transition $a \rightarrow f$. It should be mentioned that Eq. (4) can be used also in coincidence, when the gate does not influence the lifetime information as in the case of the present analysis. In Ref. [28], it is shown that taking into account the velocity distribution and DSA-effects leads to an equation for each distance x or mean end-of-flight time $\langle t_{ff} \rangle$ which reads:

$$\tau(x) = \tau(\langle t_{ff} \rangle) = \left(\tilde{R}_{af}(x) - b_{af} \sum_{h=1}^N (1 + \alpha_{ha}) \frac{I_{ha}^\gamma \tilde{S}_{af}(\infty)}{I_{af}^\gamma \tilde{S}_{ha}(\infty)} \tilde{R}_{ha}(x) \right) / \langle d\tilde{S}_{af}/dt|_{t=t_s} \rangle. \quad (5)$$

Here, the quantities I^γ are the relative intensities of the γ -ray transitions and $\tilde{S}(\infty)$ are the values of the fitted shifted decay curves at large times (i.e. where they reach constant values). The γ -ray intensities have to be known independently, indeed. However, due to the special way of gating used in the present work (see above), we had in the analysis only one feeder with an intensity balancing that of the depopulating transition. The quantities \tilde{R} are the areas of the corresponding unshifted peaks. The denominator in Eq. (5) represents the derivative $d\tilde{S}_{af}(t)/dt$ averaged over the MC-histories used for the fits of the RDDS spectra and $\tilde{S}_{af}(t)$. The final result for the lifetime is obtained by fitting a straight line through the points calculated according to Eq. (5) (the τ -curve) within the region of sensitivity where the values are reliable. Deviations of the τ -curve from a straight line in this region point to systematic errors in the analysis and give a feedback information for improvements.

To illustrate the application of the procedure, we show in Figs. 2, 3 examples of the analysis of the data for the 264 and 355 keV transitions which depopulate the $I^\pi = 4^+$ and 6^+ of the

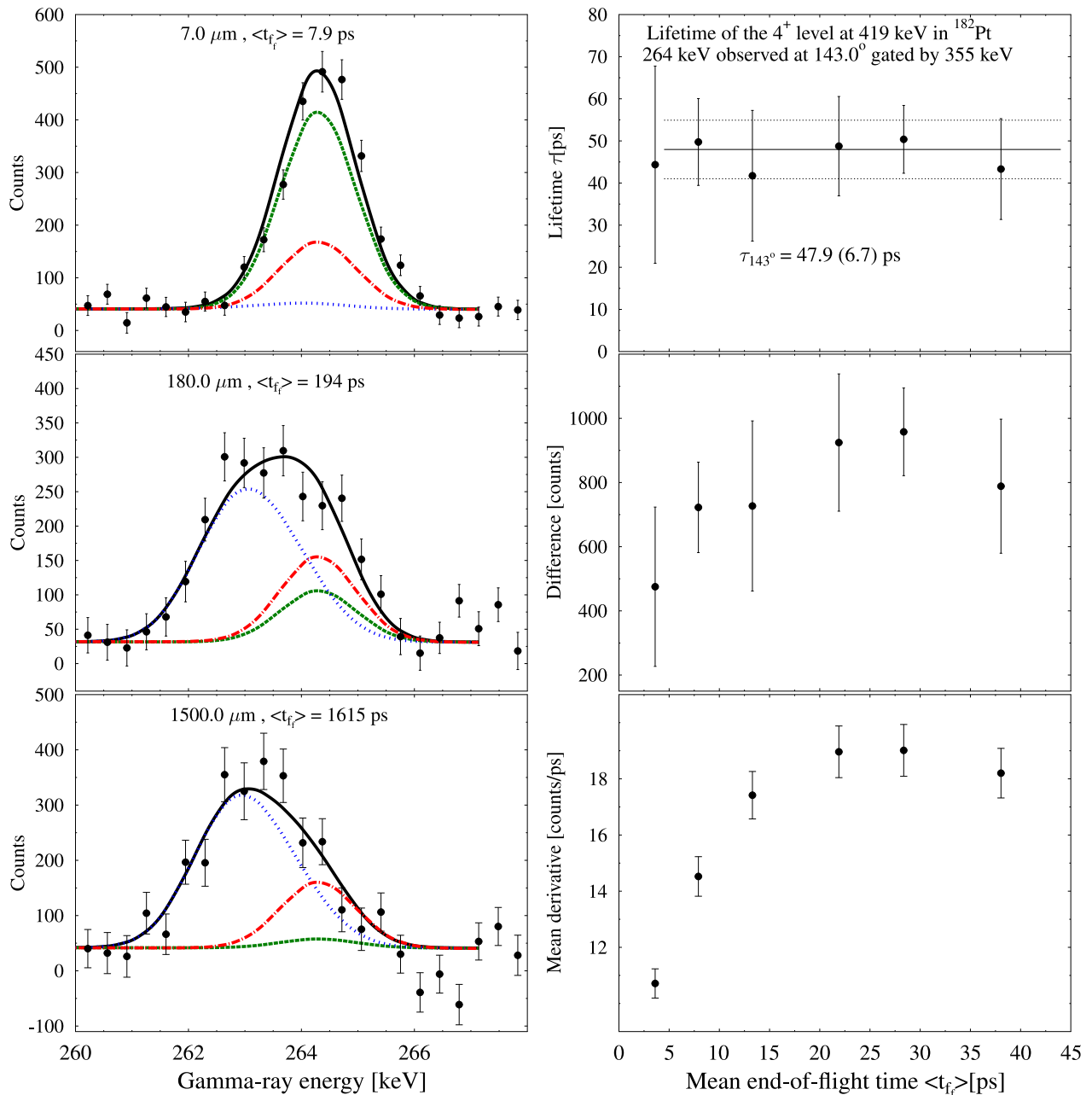


Fig. 2. Example of the lifetime analysis of the 264 keV transition. The fits in the left panels illustrate the contributions of the shifted peak (blue dotted line), unshifted peak (green short-dashed line) and decays in the target and DSA-effects (red dot-dashed line). In the top right panel, the τ -curve is displayed. It is a result of the division of the numerator in Eq. (5) (middle panel on the r.h.s) by the corresponding denominator (bottom panel on the r.h.s). See also text. (For interpretation of the references to color in this figure legend, the reader is referred to the web version of this article.)

yrast band, respectively. In the left panels of the figures, line-shapes measured at the indicated distances are displayed together with the fits at the corresponding angle. We note that the decays in the target and DSA-effects are also taken into account. The lifetime derivation is shown in the right panels. The final result for the lifetime is obtained by averaging the values derived at the different rings with paying attention to possible systematic errors (see e.g. Ref. [28]). Concerning the lifetime of the 2_1^+ level, which does not decay completely even at the larger distance measured in the present work, we used fits by a single exponential function of the areas of the corresponding unshifted peak to derive it. In Table 1, the lifetime values and the extracted $B(E2)$ transition strengths are presented.

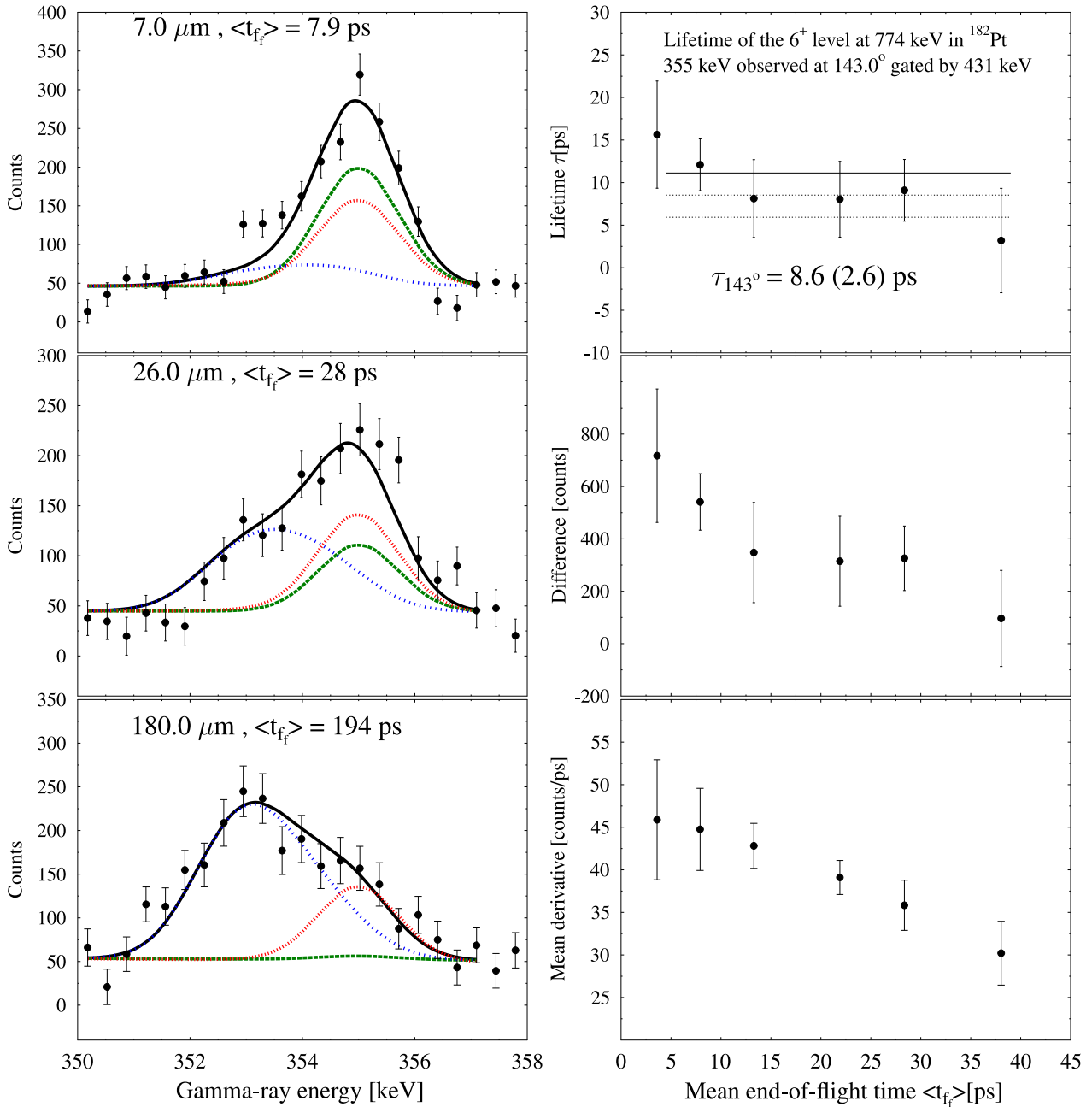


Fig. 3. Example of the lifetime analysis of the 355 keV transition. See also Fig. 2 and text.

4. Discussion

As already mentioned in Section 1, the spectroscopic properties and the shape evolution within the chain of even Pt isotopes have been considered in numerous experimental and theoretical works. However, since explicit detailed calculations for ^{182}Pt are missing in the literature, we decided to use two widely exploited models to describe the low-lying states in this nucleus and to make some conclusions about its place in the shape-transitional region. First, we employed the Interacting Boson Model-1 (IBM-1) [38] in its version called Extended Consistent Q -Formalism (ECQF) where the Hamiltonian can take the following form (see e.g. [11] and references therein)

$$H(\zeta) = c \left[(1 - \zeta) \hat{n}_d - \frac{\zeta}{4N_B} \hat{Q}^x \hat{Q}^x \right]. \quad (6)$$

Here, \hat{n}_d is the operator of the number of d -bosons, $\hat{Q}^\chi = (s^\dagger \tilde{d} + d^\dagger s) + \chi (d^\dagger \tilde{d})^{(2)}$ multiplied by the boson effective charge, e_B , yields the quadrupole operator, N_B is the number of valence bosons and c is a scaling factor. We performed a calculation of the level scheme and the $B(E2)$ transition strengths using the parameters found in a systematic study [11] and presented in Ref. [12], namely $\zeta = 0.57$ and $\chi = -0.87$ for $N_B = 13$. The normalization parameters were $c = 1.201$ and $e_B = 0.15$. For the calculation, we used an IBM code developed by P. Van Isacker [39]. The results are compared to the experiment in Fig. 4. The level energies are normalized to the energy of the 2_1^+ state and the $B(E2)$ transition strengths in the ground-state band to the $B(E2; 2_1^+ \rightarrow 0_1^+)$ value. For the side-bands where lifetimes are not known, relative $B(E2)$ branching ratios are shown. It should be mentioned that in Ref. [12] calculations with the so-called IBM plus configuration mixing model (IBM + CM) are performed, too. In this model, additional bosons (to the $N_B = 13$ for ^{182}Pt) are involved which result from the breaking of the core and are related to the intruder states. The overall Hamiltonian of the problem represents a superposition of the Hamiltonians of the two boson systems with some interaction in between. The authors [12] found that for the states up to 1.5 MeV high in excitation energy, IBM+CM gives very similar spectroscopic results to the normal IBM and therefore we do not show the results of these calculations. Other observables, as e.g. isomer and isotope shifts may be more sensitive to differences between both approaches [12,13].

The second model employed in our work is the GCM or Frankfurt model (for references see Section 1) which we present in a bit more detail. This model is based on a special case of the Bohr Hamiltonian [40], where the collective potential $V(\beta, \gamma)$ is developed in series of the quadrupole variables $\alpha_{2\mu}$ describing the oscillations of the nuclear surface. In the intrinsic frame, the potential V reads

$$V(\beta, \gamma) = \frac{1}{\sqrt{5}} C_2 \beta^2 - \sqrt{\frac{2}{35}} C_3 \beta^3 \cos 3\gamma + \frac{1}{5} C_4 \beta^4 - \sqrt{\frac{2}{175}} C_5 \beta^5 \cos 3\gamma + \frac{2}{35} C_6 \beta^6 \cos^2 3\gamma + \frac{1}{5\sqrt{5}} D_6 \beta^6. \quad (7)$$

The kinetic energy T is given by the expression

$$\hat{T} = \frac{1}{2B_2} [\hat{\pi} \times \hat{\pi}]^{[0]} + \frac{P_3}{3} \{ [[\hat{\pi} \times \alpha]^{[2]} \times \hat{\pi}]^{[0]} \} \quad (8)$$

where $\{\dots\}$ means the sum over all even permutations of $\hat{\pi}$ (the conjugated momenta) and α while B_2 is the common mass parameter. The eight parameters B_2 , P_3 , C_k ($k = 2, \dots, 6$) and D_6 are adjusted by the best fit to the experimental data (level energies, $B(E2)$ transition strengths and quadrupole moments). The Hamiltonian $H = T + V$ of the GCM is diagonalized in the basis of the five-dimensional quadrupole oscillator

$$|v\lambda\mu IM\rangle = \sum_{K=0,2,\dots}^I F_{\frac{v-\lambda}{2}}^\lambda(\beta) \Phi_K^{\lambda\mu I}(\gamma) [D_{MK}^I(\Omega) + (-)^I D_{M-K}^{I*}(\Omega)] \quad (9)$$

where the $D_{MK}^I(\Omega)$ are the Wigner functions. Detailed expressions for $F_{\frac{v-\lambda}{2}}^\lambda(\beta)$ and $\Phi_K^{\lambda\mu I}(\gamma)$ are given in Ref. [21]. The physical meaning of the quantum numbers is the following: the number of quadrupole phonons is denoted by v , λ is the number of phonons which are not coupled pairwise to angular momentum $L = 0$ and μ is the number of phonon triplets coupled to $L = 0$.

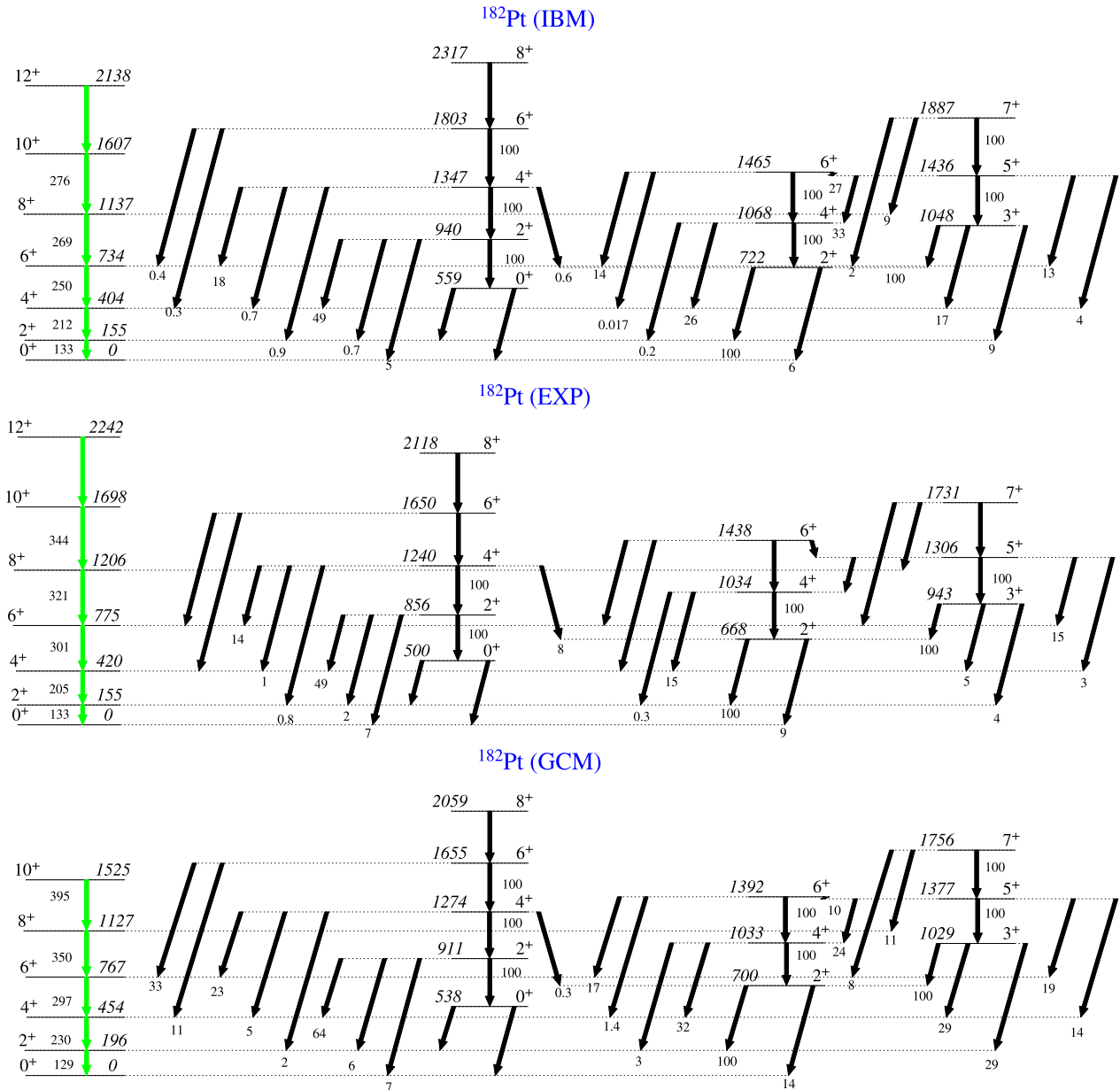


Fig. 4. Comparison of the IBM and GCM calculations with the experiment. In the ground-state band, the absolute $B(E2)$ transition strengths are shown in Weisskopf units. In the 0_2^+ and γ -bands, relative $B(E2)$ branching ratios are displayed normalized to the strongest transition (100). See also text.

The number of nodes in β of the basis wave function (Eq. (9)) is given by $n_\beta = (v - \lambda)/2$. The calculation of E2 matrix elements in the GCM is performed using the quadrupole operator

$$\hat{Q}_{2\mu} = \frac{3ZR_0^2}{4\pi} \left(\alpha_{2\mu} - \frac{10}{\sqrt{70\pi}} [\alpha \times \alpha]_{2\mu} \right). \quad (10)$$

The parameters of the GCM Hamiltonian derived from the fit of the experimental data are: $C_2 = -31.1$ MeV, $C_3 = 221.3$ MeV, $C_4 = 493.7$ MeV, $C_5 = -3576.1$ MeV, $C_6 = -1089.4$ MeV, $D_6 = 5416.5$ MeV, $B_2 = 67.98 \times 10^{-42}$ MeV s² and $P_3 = 0.0806 \times 10^{42}$ MeV⁻¹ s⁻². The results of the GCM fit are also shown in Fig. 4. As can be seen both models describe quite satisfactorily the level scheme and the transitions strengths. The IBM calculation reproduces better the yrast

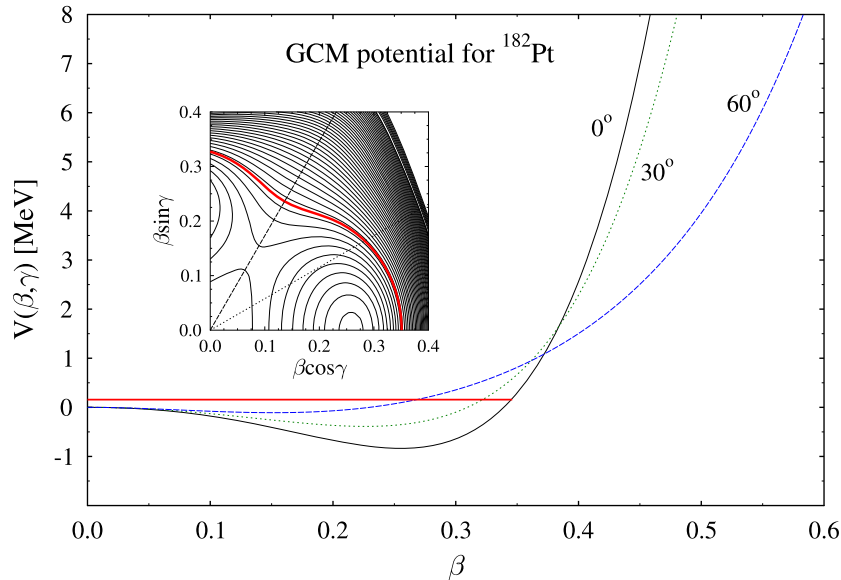


Fig. 5. Potential of the GCM for ^{182}Pt derived in the present work. The absolute ground-state energy of 0.157 MeV is represented by a thick red line. The distance between the contour levels is 0.1 MeV. See also text. (For interpretation of the references to color in this figure legend, the reader is referred to the web version of this article.)

energies and to some extent the branching ratios while the GCM gives superior results for the yrast $B(E2)$'s and the level energies of the side-bands.

Now, it is interesting to consider in more detail the nuclear shape associated with the fitted parameters of the models. In Fig. 5, we show the projections of the GCM potential (potential energy surface – PES) as well as its contour plot in the β – γ plane. From the figure, it is clear that the potential has a minimum of about -0.8 MeV on the prolate side ($\gamma = 0^\circ$, $\beta = 0.264$) and it is characterized by a considerable γ -softness with a saddle point on the oblate ($\gamma = 60^\circ$) axis. This picture is in agreement with many calculations (see e.g. Refs. [3,4,41]) of the nuclear shape for the Pt isotopic chain, where a shape transition occurs between ^{188}Pt and ^{186}Pt , and lighter Pt nuclei have a prolate ground-state band. Using the transition quadrupole moment for the $2_1^+ \rightarrow 0_1^+$ transition in Table 1 and the relation [43]

$$Q_0 = \frac{3}{\sqrt{5\pi}} Z R_0^2 \beta (1 + 0.16\beta), \quad (11)$$

we derive $\beta_{\text{exp}} = 0.25(2)$ for the experimental mean value of the quadrupole deformation of the charge distribution. According to Ref. [44], due to the difference between the nuclear charge distribution and the mean field, $\beta \approx 1.1 \beta_{\text{mean-field}}$, and we obtain $\beta_{\text{mean-field}} = 0.23(2)$ for the deformation of the ground-state band of ^{182}Pt . This value coincides with the predictions of a calculation by R. Wyss et al. [4], where the authors infer also some hexadecapole deformation of $\beta_4 = -0.017$. The shape of the GCM potential derived in the present work is in a good agreement with recent mean field studies of the structural changes in the Pt isotopes (cf. Figs. 2–4 in Ref. [45]). K. Nomura et al. [46] have performed spectroscopic calculations for the description of the shape transition in the Pt isotopes using the Hamiltonian of the proton–neutron IBM-2 derived from Hartree–Fock–Bogoliubov calculations with the Gogny energy density functional. The potential energy surface of the IBM-2 derived for ^{182}Pt is in good qualitative agreement with the presently obtained PES of the GCM. It should be mentioned that the positions of the potential minimum on the prolate axis in practice coincide (cf. Fig. 5 and Fig. 1 in [46]).

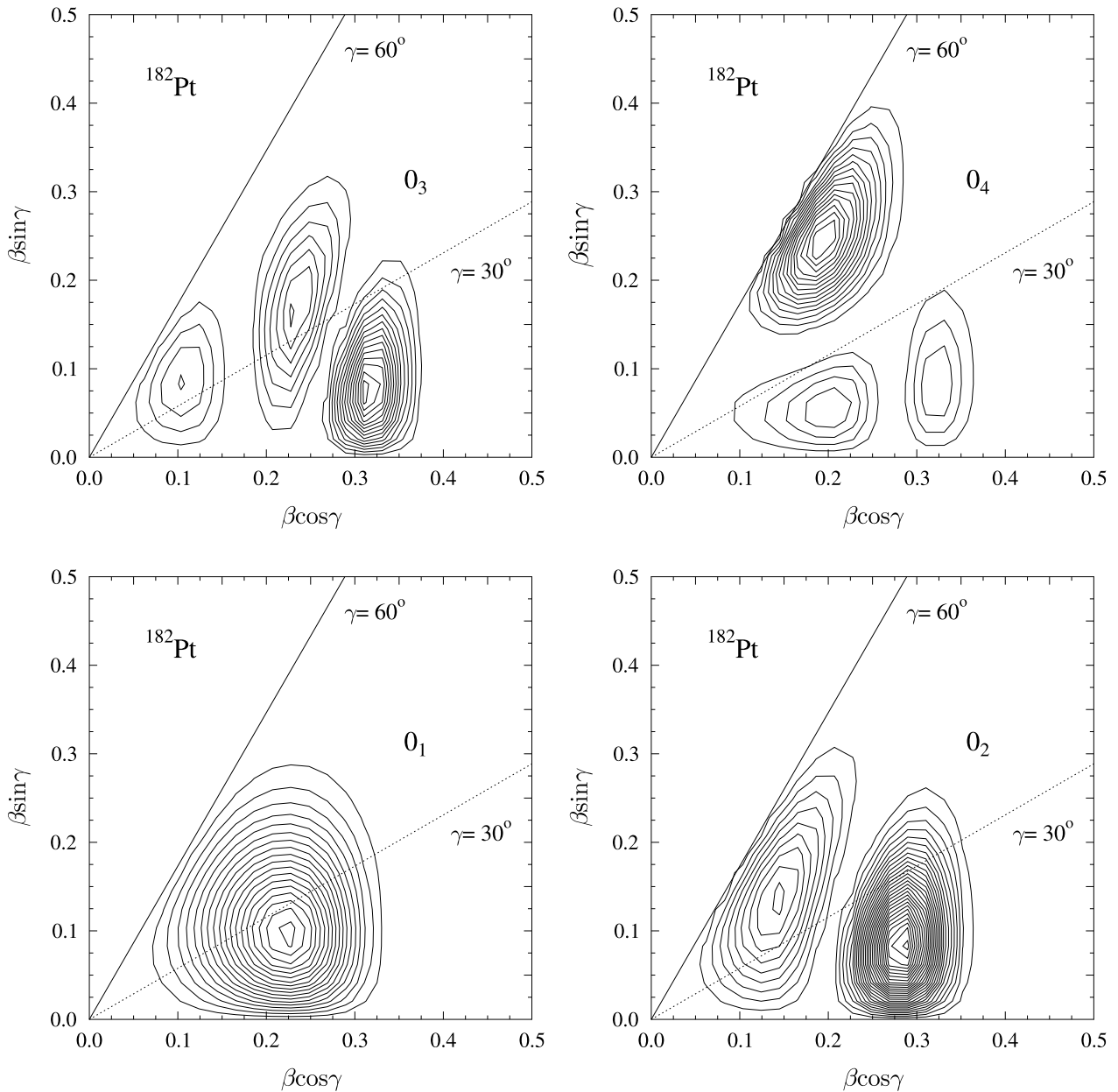


Fig. 6. Probability distributions in the β - γ plane of the wave functions of the first four 0^+ states in ^{182}Pt according to the GCM.

Because β and γ are dynamic variables in the GCM, the maximum of their probability distribution (the squared wave function multiplied by the volume element $\beta^4 \sin(3\gamma)$) does not necessarily coincide with the potential minimum. Thus, we show in Fig. 6 these distributions for the first four 0^+ states. The 0_3^+ state lies at 1.230 MeV and the 0_4^+ state at 1.339 MeV, respectively. Obviously, the 0_2^+ state can be interpreted as a β -vibration, its probability distribution has roughly one node in β . We remind the reader that the number of nodes of the basis functions in Eq. (9) is fixed and its mean value can be calculated for every state (see also Ref. [47]). According to the GCM, this number is similar and close to 1 for the states of the 0_2^+ band. On the other hand, Fig. 6 suggests that this band is characterized by two composing components: one prolate, more deformed than the 0_1^+ band structure, and one more triaxial to oblate, less deformed structure. Similar observations for a multi-component structure can be made also for the other, higher-lying 0^+ states. They indicate a mixing between these states, where the 0_4^+ state is

Table 2

Comparison of some characteristic energy and $B(E2)$ ratios calculated in the framework of X(5), IBM and GCM with experiment. The X(5) 2_2^+ and 4_2^+ states belong to the $s = 2 0^+$ band and have to be compared with the experimental 2_3^+ and 4_3^+ level, respectively. The transitions between states with equal spins have a mixed multipolarity. See also text and Fig. 4.

Ratio	Experiment	X(5)	IBM	GCM
$(E_{4_1^+} - E_{0_1^+})/(E_{2_1^+} - E_{0_1^+})$	2.71	2.91	2.61	2.32
$(E_{6_1^+} - E_{0_1^+})/(E_{2_1^+} - E_{0_1^+})$	5.00	5.45	4.74	3.92
$(E_{0_2^+} - E_{0_1^+})/(E_{2_1^+} - E_{0_1^+})$	3.22	5.67	3.61	2.75
$(E_{4_2^+} - E_{0_2^+})/(E_{2_2^+} - E_{0_2^+})$	2.08	2.79	2.07	1.97
$B(E2; 2_2^+ \rightarrow 4_1^+)/B(E2; 2_2^+ \rightarrow 0_2^+)$	0.49(15)	0.46	0.49	0.64
$B(E2; 2_2^+ \rightarrow 2_1^+)/B(E2; 2_2^+ \rightarrow 0_2^+)$	≤ 0.02	0.11	0.007	0.058
$B(E2; 2_2^+ \rightarrow 0_1^+)/B(E2; 2_2^+ \rightarrow 0_2^+)$	0.07(1)	0.03	0.05	0.07
$B(E2; 4_2^+ \rightarrow 6_1^+)/B(E2; 4_2^+ \rightarrow 2_2^+)$	0.14(5)	0.23	0.18	0.23
$B(E2; 4_2^+ \rightarrow 4_1^+)/B(E2; 4_2^+ \rightarrow 2_2^+)$	≤ 0.01	0.05	0.007	0.045
$B(E2; 4_2^+ \rightarrow 2_1^+)/B(E2; 4_2^+ \rightarrow 2_2^+)$	0.008(2)	0.008	0.009	0.022

characterized by a nearly oblate shape. In this sense, the GCM predicts a shape coexistence in ^{182}Pt in the framework of a mixing of bands with different quadrupole deformation, confirming earlier experimental findings (e.g. [8]) for the light Pt isotopes. This shape coexistence is not necessarily related to a PES with distinct and isolated different local minima. It is interesting to note that a recent study [42] of ^{192}Pt , investigating the nature of the 0^+ excitations, suggests that the 0_4^+ state in that nucleus is an intruder state, probably with an oblate deformation.

Since the introduction [22] by Iachello of the benchmark X(5) model, many experimental and theoretical efforts have been dedicated to the investigation of the shape/phase transition between spherical vibrator (U(5) limit of the IBM) and axially deformed prolate rotor (SU(3)). Examples of this phenomenon have been discovered in $N = 90$ nuclei from the $A = 150$ mass-region (^{150}Nd [48], ^{152}Sm [49], ^{154}Gd [50]). Later, it was also found in some Os nuclei with $A \approx 180$, and is best established in ^{178}Os [23]. In the vicinity of $Z = 82$, one may expect that if the X(5) shape transition occurs in the osmiums ($Z = 76$), than the nearby lying W nuclei should have a more rotor-like behavior, while the corresponding Pt nuclei should display a more vibrational character. In the light of the previous discussion, this picture oversimplifies the real development of the shape changes in the Pt isotopes, where different nuclear ground-state shapes are suggested to occur (spherical for N approaching 126, oblate and triaxial for smaller neutron number, prolate below ^{188}Pt , etc.). In the majority of the cases, the calculated PES surfaces are characterized by a significant γ -softness. Additionally, these ground-state shapes coexist with differently deformed excited states. Nevertheless, it is possible that remnants from the X(5)-structure persist in ^{182}Pt , and below we investigate this effect. In Fig. 7, we present the experimental $B(E2)$ transition strengths in the ground-state band compared to model calculations. The best description is provided by the GCM and X(5) followed by the IBM. This could be an indication that ^{182}Pt has an X(5) character. However, this is a premature conclusion as revealed by the comparison in Table 2 of some energy and $B(E2)$ ratios calculated within that model and experiment. The main discrepancy is the position of the 0_2^+ state, which is about two times higher in X(5) compared to the experiment. As discussed above, this state is related to the effects of shape

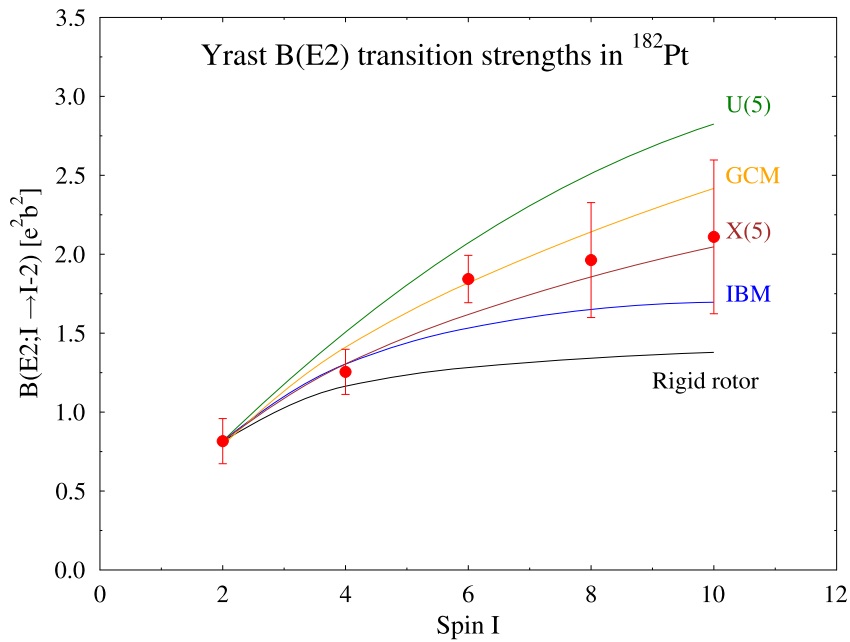


Fig. 7. Transition strengths in the yrast band of ^{182}Pt . The different theoretical models used are indicated. With the exception of the GCM, all models are normalized to the $B(E2)$ value for the $2_1^+ \rightarrow 0_1^+$ transition. In the case of X(5), the numerical values are taken from Ref. [51].

coexistence and configuration mixing, and cannot be described by the benchmark model. Nevertheless, the present results for the $B(E2)$ transition strengths in the ground-state band may be interpreted as an indication that some X(5) features persist in ^{182}Pt coexisting with excitations corresponding to different nuclear shapes. This is corroborated also by the experimental $B(E2)$ branchings of the transitions from the 0_2^+ side band to the ground-state band where for instance the $B(E2, I \rightarrow I+2)$ transition strengths dominate over the $B(E2, I \rightarrow I)$ and $B(E2, I \rightarrow I-2)$ ones. In Table 2 we include also the results of the calculations with the IBM and GCM. The latter models describe better than X(5) the experimental energy and $B(E2)$ ratios. More precisely, the IBM provides a very good description of the energy ratios and the $B(E2)$ branching ratios from the 2_3^+ and 4_3^+ levels of the 0_2^+ band. Theoretical values for U(5) and the rigid rotor model are not included because they are ruled out by the yrast $B(E2)$'s. The exact position of ^{182}Pt in the IBM parameter space and its closeness to the shape/phase transitional region may be found in Fig. 4 of Ref. [11]. In that figure, the Pt isotopes from $A = 176$ to 194 are positioned in the Casten triangle, and ^{182}Pt lies very close, but not in the X(5) transitional region. It deviates somewhat toward the O(6) vertex of the triangle, indicating the importance of the γ -softness effects.

5. Conclusions

Five lifetimes in the yrast band of ^{182}Pt have been determined for the first time using the Recoil Distance Doppler-Shift Method. To analyse the data and overcome difficulties, a special new version of the Differential Decay Curve Method has been employed. Calculations within the frameworks of the Interacting Boson Model and the General Collective Model have been performed. The calculations indicate shape phase transition in the investigated nucleus and confirm earlier findings in the light Pt isotopes. The Potential energy surface of the GCM derived in the present work is in agreement with previous theoretical calculations. The behaviour of the $B(E2)$ transition strengths in the yrast band reveals X(5) features of this band coexisting with side-bands with different quadrupole deformations. To investigate further these structures, in-

traband and interband transition strengths in the side bands have to be experimentally known. Lifetime measurements in neighboring $^{178,180}\text{Pt}$ are also highly desirable.

Acknowledgements

K.A.G and P.P. would like to thank the colleagues from the University of Cologne for their kind hospitality. This work was supported by the Deutsche Forschung Gemeinschaft (DFG) within the East-European–Germany collaboration program and contracts Nos. Jo 391/8-1 and Jo 391/11-1. The authors are also indebted for the support by the partnership agreement between the University of Cologne and University of Sofia and by the BgNSF under Contract No. DO 02-219.

References

- [1] J.L. Wood, K. Heyde, W. Nazarewicz, M. Huyse, P. Van Duppen, *Phys. Rep.* 215 (1992) 101.
- [2] A.N. Andreyev, et al., *Nature* 405 (2000) 430.
- [3] R. Bengtsson, T. Bengtsson, J. Dudek, G. Leander, W. Nazarewicz, J. Zhang, *Phys. Lett. B* 183 (1987) 1.
- [4] R. Wyss, W. Satula, W. Nazarewicz, A. Johnson, *Nucl. Phys. A* 511 (1990) 324.
- [5] H.C. Chiang, S.T. Hsieh, *Nucl. Phys. A* 472 (1987) 202.
- [6] M.K. Harder, K.T. Tang, P. Van Isacker, *Phys. Lett. B* 405 (1997) 25.
- [7] I.O. Morales, A. Frank, C.E. Vargas, P. Van Isacker, *Phys. Rev. C* 78 (2008) 024303.
- [8] G.D. Dracoulis, A.E. Stuchbery, A.P. Byrn, A.R. Poletti, S.J. Poletti, J. Gerl, R.A. Bark, *J. Phys. G: Nucl. Phys.* 12 (1986) L97.
- [9] U. Garg, et al., *Phys. Lett. B* 180 (1986) 319.
- [10] P.M. Davidson, G.D. Dracoulis, T. Kibedi, A.P. Byrne, S.S. Anderssen, A.M. Baxter, B. Fabricius, G.J. Lane, A.E. Stuchbery, *Nucl. Phys. A* 657 (1999) 219.
- [11] E.A. McCutchan, R.F. Casten, N.V. Zamfir, *Phys. Rev. C* 71 (2005) 061301, (R).
- [12] J.E. Garcia-Ramos, K. Heyde, *Nucl. Phys. A* 825 (2009) 39.
- [13] J.E. Garcia-Ramos, V. Hellemans, K. Heyde, *Phys. Rev. C* 84 (2011) 014331.
- [14] D.G. Popescu, et al., *Phys. Rev. C* 55 (1997) 1175.
- [15] B. Singh, J.C. Roediger, *Nuclear Data Sheets* 111 (2010) 2081.
- [16] A. Dewald, S. Harissopulos, P. von Brentano, *Z. Phys. A* 334 (1989) 163.
- [17] G. Böhm, A. Dewald, P. Petkov, P. von Brentano, *Nucl. Instr. Meth. Phys. Res. A* 329 (1993) 248.
- [18] D. Troltenier, J.A. Maruhn, W. Greiner, V. Velazquez Aguilar, P.O. Hess, J.H. Hamilton, *Z. Phys. A* 338 (1991) 261.
- [19] D. Troltenier, J.A. Maruhn, P.O. Hess, in: K. Langanke, J.A. Maruhn, S.E. Koonin (Eds.), *Computational Nuclear Physics*, Springer, Berlin, 1991, p. 105.
- [20] G. Gneuss, W. Greiner, *Nucl. Phys.* 171 (1971) 449.
- [21] P.O. Hess, J.A. Maruhn, W. Greiner, *J. Phys. G: Nucl. Phys.* 7 (1981) 737.
- [22] F. Iachello, *Phys. Rev. Lett.* 87 (2001) 052502.
- [23] A. Dewald, et al., *J. Phys. G: Nucl. Part. Phys.* 31 (2005) S1427.
- [24] A. Dewald, et al., *Nucl. Phys. A* 545 (1992) 822.
- [25] J. Eberth, H.G. Thomas, P. von Brentano, R.M. Lieder, H.M. Jäger, H. Kämmerling, M. Berst, D. Gutknecht, R. Henck, *Nucl. Instr. Meth. Phys. Res. A* 369 (1996) 135.
- [26] T.K. Alexander, J.S. Forster, *Adv. Nucl. Phys.* 10 (1978) 197.
- [27] P. Petkov, D. Tonev, J. Gableske, A. Dewald, T. Klemme, P. von Brentano, *Nucl. Instr. Meth. Phys. Res. A* 431 (1999) 208.
- [28] P. Petkov, et al., *Nucl. Phys. A* 674 (2000) 357.
- [29] G. Goldring, in: R. Bock (Ed.), *Heavy Ion Collisions*, vol. 3, North-Holland Publishing Company, 1982, p. 484.
- [30] G. Winter, *ZfK Rossendorf Report*, ZfK-497, 1983;
G. Winter, *Nucl. Instr. Meth.* 214 (1983) 537.
- [31] P. Petkov, et al., *Nucl. Phys. A* 640 (1998) 293.
- [32] W. M Currie, *Nucl. Instr. Meth.* 73 (1969) 173.
- [33] J. Lindhard, M. Scharff, H.E. Schiøtt, *Kgl. Dan. Vid. Selsk. Mat. Fys. Medd.* 33 (14) (1963).
- [34] L.C. Northcliffe, R.F. Schilling, *Nucl. Data Tables A* 7 (1970) 233.

- [35] J.F. Ziegler, W.K. Chu, Atomic Data Nucl. Data Tables 13 (1974) 463.
- [36] J.F. Ziegler, J.P. Biersack, in: D.A. Bromley (Ed.), Treatise on Heavy-Ion Science, vol. 6, Plenum Press, 1985, p. 95.
- [37] J. Keinonen, in: S. Raman (Ed.), Capture Gamma-Ray Spectroscopy and Related Topics-1984, Proceedings of the Fifth International Symposium, Knoxville, Tennessee, in: AIP Conf. Proc., vol. 125, AIP, New York, 1985, p. 557.
- [38] F. Iachello, A. Arima, The Interacting Boson Model, Cambridge University Press, Cambridge, England, 1987.
- [39] P. Van Isacker, private communication.
- [40] A. Bohr, B.R. Mottelson, Nuclear Structure, vol. 2, Benjamin, New York, 1975.
- [41] M. Veskovic, M.K. Harder, K. Kumar, W.D. Hamilton, J. Phys. G: Nucl. Phys. 13 (1987) L155.
- [42] E.A. McCutchan, R.F. Casten, V. Werner, R. Winkler, R.B. Cakirli, G. Gürdal, X. Liang, E. Williams, Phys. Rev. C 78 (2008) 014320.
- [43] A. Bohr, B.R. Mottelson, Dan. Mat.-Fys. Medd. 30 (1) (1955).
- [44] W. Nazarewicz, M.A. Riley, J.D. Garrett, J. Dudek, Nucl. Phys. A 512 (1990) 61.
- [45] R. Rodriguez-Guzman, P. Sarriguren, L.M. Robledo, J.E. Garcia-Ramos, Phys. Rev. C 81 (2010) 024310.
- [46] K. Nomura, T. Otsuka, R. Rodriguez-Guzman, L.M. Robledo, P. Sarriguren, Phys. Rev. C 83 (2011) 014309.
- [47] P. Petkov, A. Dewald, W. Andrejtscheff, Phys. Rev. C 51 (1995) 2511.
- [48] R. Krücken, et al., Phys. Rev. Lett. 88 (2002) 232501.
- [49] R.F. Casten, N.V. Zamfir, Phys. Rev. Lett. 87 (2002) 052503.
- [50] D. Tonev, A. Dewald, T. Klug, P. Petkov, J. Jolie, A. Fitzler, O. Möller, S. Heinze, P. von Brentano, R.F. Casten, Phys. Rev. C 69 (2004) 034334.
- [51] D. Bonatsos, D. Lenis, N. Minkov, P.P. Raychev, P.A. Terziev, Phys. Rev. C 69 (2004) 014302.